Critical current densities of bicrystalline HTSC film under various magnetic fields

S. M. Lim, Y.Jung, K.Jang, S.M.Lee, Y.H.Jung, and D. Youm

Physics Department, KAIST, 305-701 Daejon, Korea

ariella@mail.kaist.ac.kr

Abstract-- **Critical current densities were measured for a bicrystalline $(Sm_{0.8}Dy_{0.2})Ba_2Cu_3O_7$ film under various magnetic fields ($\overline{H}_a$). The fields were varied from $-0.7KOe$ to $+0.7KOe$ for various orientations with respect to the film surface. The curves of the critical current densities (J_{cb}) vs $\overline{H}_a$ showed the well known butterfly-like hysteretic curves. Our data could be analyzed for the two components of field, which are normal and parallel to the film surface, respectively. We combined the effect of $H_\perp$ deduced from the data for the normal field ($\theta = 90°$) and the effect of $H_\parallel$ deduced from the data for the almost parallel field ($\theta = 2°$). Our analyses indicate that J_{cb} depends on the two components of flux density at the grain boundary. All the experimental data for various θ s fit well to this new formula which was obtained by multiplying the factors deduced from the field dependences of these two components.**

1. INTRODUCTION

Coated conductors (CCs) consist of numerous grain boundaries (GB) of small mis-orientation angles [1]. Thus the effects of GBs on the properties of CCs are important. Most of electro-magnetic properties of CCs are determined by motion of vortices, while the roles of the vortices at intra-grains, Abrikosov (A-) vortices, are different from those of the vortices at GBs, Josephson (J-) vortices. Since J-vortices are more weakly pinned than A-vortices, the critical current densities are determined by the motions of J-vortices for the currents crossing GBs. The voltage is proportional to the product of the density and the speed of the J-vortices, which move along GB. They are closely related to the local distributions of vortices and currents, respectively.

The basic properties of critical current densities in the bicrystalline films of various materials with various mis-orientation angles are well-known[2]. For the fields applied in the normal direction of the film surfaces, J_{cb} vs $\overline{H}_a$ can be described by salient hysteretic curves. This indicates hysteretic changes of vortex distribution around GB, which can be well explained by the theory of E. H. Brandt [3]. The physical concept can be briefly described as following [2]. Lorentz force for critical condition is limited by fixed density of pinning centers and proportional to the critical current density times the vortex density.

Hence J_{cb} decreases as vortex density increases. Since magnetic flux is distributed according to the critical state of A-vortices, $\overline{H}_a$ induces appropriate distributions of both critical currents and Meissner currents in the film [3]. The local field around GB, which determines the local density of J-vortices, can be obtained from the distributions of these currents using the mathematical formula in Brandt model [3]. We can take the edge field in the Brandt formula for the approximated expression of the local field at GB. The hysteretic behavior of J-vortex density is due to the fact that the fields around GB, which form a spike focused at GB, always change in advance to $\overline{H}_a$.

In this paper we report our experimental studies, which were similar to the previous ones but under extended conditions, i.e. obliquely applied fields. We measured J_{cb} vs $\overline{H}_a$ of a bicrystalline film as functions of the magnitude of field, H_a for various θ s, while θ is the angle between the direction of $\overline{H}_a$ and the film surface. The geometry of our sample and measurement parameters is given in the inset of Fig.1. The angle, θ, was varied from 2° to 90° The flux lines of J-vortices are virtually normal to the film surface because they are positioned in the planar defects, GBs. However, when θ is zero, $\overline{H}_a$ becomes parallel to the applied current as shown in the inset of Fig.1. The vortices produced by the parallel $\overline{H}_a$ are in the plane of film and parallel to the applied currents. There are no Lorentz forces between the currents and those types of vortices. Generally, the oblique field has both a parallel component and a normal component, while the normal component ($H_\perp$) produces J-vortices. It is expected that the roles of these two components might be different. In this paper, we report the experimental studies for the effects of $H_\perp$ described by Brandt theory and also the effects of $H_\parallel$ described by Bean model.

2. EXPERIMENTS

A c-axis normal thin film of $(Sm_{0.8}Dy_{0.2})Ba_2Cu_3O_7$ was deposited on a bicrystalline $SrTiO_3$ substrate of 30°-symmetric mis-orientation angle of GB using co-evaporation method [4]. The film was ~300nm thick and

5mmx10mm rectangular with a 5mm long GB. The sample geometry is shown in the inset of Fig.1. The zero-resistance temperature, T_c, was 92K. We measured I-V curves using four probe methods under the fields, $\overline{H}_a$, which were applied in various directions. The magnitude of field, H_a, was varied cyclically within the range of $-0.7KOe \sim +0.7KOe$ with fixed θ s; 2°, 22.5°, 45°, 67.5°, and 90°. When θ is 90°, the magnetic field is normal to the film surface, and when θ is 2°, the field is almost parallel to the plane of the film and normal to GB as shown in the inset of Fig.1. The measurements were done at the temperature, 77K.
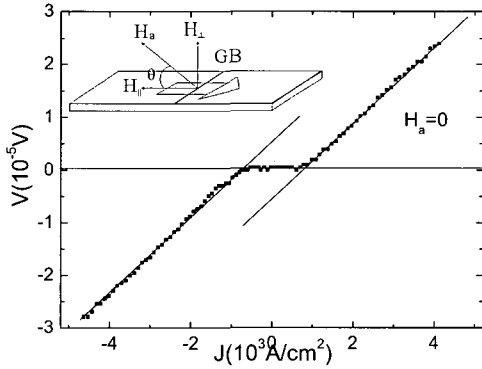

Fig. 1. Method of estimation of J_{cb} from typical I-V curve. The best-fit straight lines are shown. Using the extrapolations of the two straight lines, the two intersection points with the x-axis are found. J_{cb} is the half distance between the two points. Inset: Schematic diagram for the geometry of the sample and the measurement parameters; θ is the angle between the direction of $\overline{H}_a$ and the film surface, which was varied from 2° to 90°. The center-line is GB. The current applied across GB and J-vortices at GB are shown.

We estimated J_{cb} from each I-V curve using the extrapolation of the straight lines which were obtained by the best fitting to the data points as shown in Fig.1. The salient straight lines in the I-V curves enabled us to find the best-fit J_{cb} which is a half distance between the two intersection points of the straight lines and the x-axis. Fig.2a, 2b, 2c, 2d, and 2e show J_{cb} vs H_a for the five cases of $\theta = 2°$, 22.5°, 45°, 67.5°, and 90°. Each of them shows the well-known hysteretic curves with two peaks as shown in Ref 2 except the curve for $\theta = 2°$ which shows very broad peaks. The values of J_{cb} at the peak points for all the curves except $\theta = 2°$ are very similar but the values of H_a at the peak points (H_a^*) are different.

Fig.3 shows H_a^* as a function of θ in order to clarify the differences. Here H_a^* was estimated from the center line of the peak shape. On the other hand, the values of J_{cb}

around the tails ($H_a = \pm0.7KOe$) for all the curves except $\theta = 2°$ are similar. The values of J_{cb} at $H_a = 0$ for crossing points of the butterfly curves for all data including $\theta = 2°$ are similar as to be $\sim 0.3 \times 10^3 A/cm^2$. In the figure, the arrows indicate the direction of sequential acquisitions of data point, which follow the butterfly-like curves. These features are similar to our previous results, which were obtained for the fields applied in normal direction [2]. However we will study the details of differences, which might be due to the obliquity of fields.
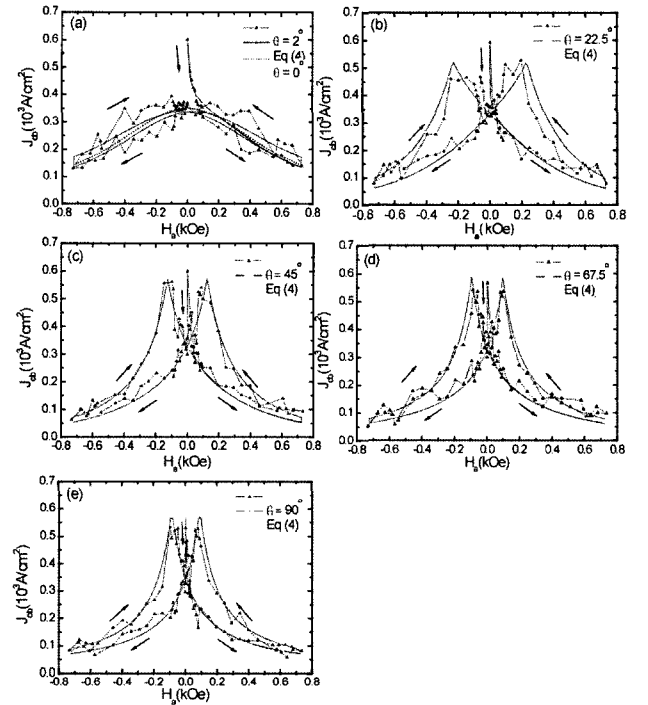

Fig. 2. J_{cb} vs H_a for the five cases; (a)$\theta = 2°$, (b)22.5°, (c)45°, (d)67.5°, and (e)90°. The arrows indicate the direction of sequential acquisitions of data points, which follow the butterfly-like curves. The solid line in each figure is obtained by the calculation using Eq.(4).
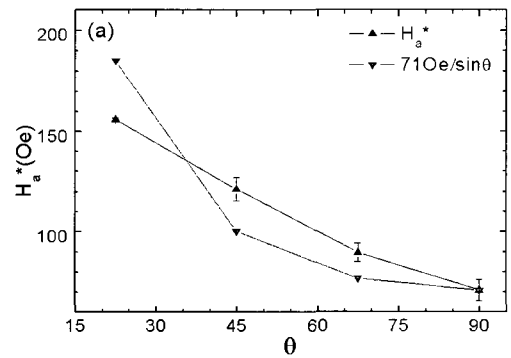

Fig. 3. Values of H_a^* at the peak points vs θ, which clarify their differences. Here, the value of H_a^* at each peak was estimated from the center line of the shape of the peaks.

All the data except $\theta = 2°$ are plotted again as functions of the normal component of fields, $H_\perp = H_a \sin\theta$ in order to clarify the differences and the similarities between the data for different θ s. The reason for the omission of the case of $\theta = 2°$ is the difficulty of plotting with $H_\perp = H_a \sin\theta \approx 0$ for $\theta = 2°$. The important feature of these data can be summarized as following. (1) The values of $H_\perp$ for the peak positions of all the curves except $\theta = 2°$ are similar as shown in Fig.3. The inset-a is a plot of H_a^* as functions of θ. The inset-a also shows the plot of $71Oe / \sin\theta$ as a function of θ, where $71Oe$ is H_a^* for the peak of $\theta = 90°$. The two curves are roughly coincident, which means $H_a^* \sin\theta \approx 71Oe$ for the peaks of various θ s. In other words, the values of $H_\perp^* = H_a^* \sin\theta$ are almost the same as $71Oe$. This implies that $H_\perp$ is a meaningful variable for fields, which affects the properties of vortex behaviors. This is easy to understand because the J-vortices density is produced by $H_\perp$ (not $H_\parallel$) because the flux lines of J-vortices in the plane of GB is virtually normal to the film surface. As explained in Ref.3, the position of peak, $H_\perp^*$, is given by the intra-grain critical current density, J_{cg}, which is the same for all the data. (2) However, when the fields are increased above the peak points, the curves as functions of $H_\perp$ show diversity of decreasing rates. This indicates that the magnitude of J_{cb} depends on the variable other than $H_\perp$ because $H_\perp$ s are the same for all the curves as expressed by the common x-axis in this figure. The other variable should be $H_\parallel$. Here, $H_\parallel = H_a \cos\theta$ is the parallel component of $\vec{H}_a$. In other words, J_{cb} seems to depend on $H_\parallel$ as well as $H_\perp$. The details of this will be described later. (3) In Fig.2a, the curve for $\theta = 2°$ also shows the strong field dependence of J_{cb}. $\vec{H}_a$ is almost parallel to the film surface. This clearly implies that $H_\parallel$ also causes the reduction of J_{cb}. This curve also shows small hysteresis with somewhat different curve pattern.

We will discuss these features as relating them with the roles of $H_\perp$ and $H_\parallel$ for the behaviors of J-vortices. We will show the method to unify the features of data including their differences and similarities for any θ s in the next section.

3. ANALYSES OF EXPERIMENTAL RESULTS

We take the theories in the Brandt's two papers for a strip film as the standard ones for the analyses of our data [3][5]. We assume that the field intensity near GB of bicrystalline film might show the behaviors similar to the edge field of a single strip film, which was formalized in Brandt model [3]. This is the same as the method used in our previous paper [2]. According to one of the Brandt's

papers for obliquely applied fields, the effects of the two components, $H_\parallel$ and $H_\perp$, can be separable for thin film samples [5]. The field distribution and the current distribution for $H_\perp$ are given by Brandt model described in the other paper [3]. The field distribution and the current distribution for $H_\parallel$ are given by Bean model because the film sample is a kind of thin slab. Since the net current integrated over film thickness in Bean model vanishes, the distribution of the total current, which is the current integrated over the film thickness, is not affected by $H_\parallel$ and consequently determined by $H_\perp$ only. Moreover, since the currents near edge is always saturated by small $H_\perp$, there is no screening for $H_\parallel$. Hence the edge fields are obtained by superposition of the field induced by $H_\perp$ and $H_\parallel$ itself as shown in Fig.4 [5]. This will be explained in detail later.

The key points of the data can be summarized as following.

(1) Initial drops of J_{cb}

All the five curves in Fig.2 show the initial sharp drops of J_{cb} as H_a is increased from zero at first[6] and then they show the butterfly-like hysteretic curves repeatedly. The changes of J_{cb} for the hysteretic curves are much slower than the initial drops. As H_a varies repeatedly in the range of $-0.7KOe \sim +0.7KOe$, J_{cb} changes in the closed curve of the butterfly. Hence, the initial drop and the butterfly-like curves seem to be two distinct phenomena. At the very initial zero field without any previous history of field, J_{cb} s in the data of any θ s are $\sim 0.6 \times 10^3 A/cm^2$ and then undergo extremely sharp drops down to the half value, $\sim 0.3 \times 10^3 A/cm^2$, as the field increases by few Gausses. According to Brandt model, the field distribution forms a spike at the edge or GB with focusing effect (see Fig.4d). This causes the sharp increase of J-vortex density at GB under initial small value of H_a, which results in the initial sharp drops of J_{cb}.

(2) Parallel components and normal components of fields

First of all, one might consider the multi-component theory, which is meaningful only when the applied currents are as large as the screening currents due to the applied fields [7]. However, in our cases, the applied currents across GB are much smaller than the screening currents. J_{cb} is at least ~ 2 order of magnitude smaller than J_{cg} in our bi-crystalline sample and the current applied across GB($\propto J_{cb}$) is negligible in comparison with the shielding current($\propto J_{cg}$)[2]. Thus, the multi-component theory is irrelevant.

When the oblique $\vec{H}_a$ is applied, the two components of field, $H_\perp$ and $H_\parallel$, should be considered. Only $H_\parallel$ is non zero for $\theta = 0°$ and only $H_\perp$ is non zero for $\theta = 90°$. For

the case of $\theta = 90°$, we already reported lots of experimental results and relevant analyses, which were well explained by the Brandt model. For $\theta = 0°$, Bean model is useful[8]. For oblique fields, one must consider both Brandt model for $H_\perp$ and Bean model for $H_\parallel$. Since both models are based on the critical state model with common critical currents, it is not simple to combine the two models. The details of current and field distributions in the film are well described in Ref.5. Fortunately the edge-fields are simple because there is no core near edges or GB as shown in Fig.4b, which is the cross-sectional view of the current distribution and the two cores. Fig4a is the top view of the currents and vortex distributions in the sample. All the schematic diagrams in Fig.4 are valid for the fields increased from zero without previous history. There are no vortices and no currents in the cores which are formed in the two Meissner regions[5]. According to Ref.5, the currents near edges or GB are simply saturated as $J(y) = DJ_{cg}$ as shown in Fig.4c and are determined sorely by Brandt model for $H_\perp$. Here $J = J_+ + J_-$, which is integration of currents density over film thickness. The cross-sectional distributions of current density in Fig.4b are homogeneous as $\pm J_{cg}$ except the core regions. The

screening current for $H_\parallel$ is $J_B = \frac{1}{2}(J_+ - J_- - |J|)$, and

vanishes around GB and edges as shown in Fig.4c. Hence there are no screening effects at GB for additional $H_\parallel$[5]. Moreover, the net amount of screening current induced by $H_\parallel$ in the full thickness of film of any regions is zero because the current consists of $+J_B$ and $-J_B$ from Bean model. Hence, $H_\parallel$ gives no effects on the total amount of local current(J) in the full thickness of film, so the edge field of Brandt model for $H_\perp$ is basically valid even with $H_\parallel$[5]. Hence, the fields at GB is the superposition of the normal field and parallel field, while the normal field is determined sorely by the Brandt formula for $H_\perp$ and the parallel field is $H_\parallel$ itself [5] because the parallel component of the field given by Brandt model vanish at GB by the symmetry for $\pm y$ [3]. The y-axis is defined in Fig.4a. The distributions of the normal component ($B_\perp$) and the parallel component ($B_\parallel$) of flux density integrated over film thickness are shown in Fig.4d.[2][3][5]

Since the plane of GB defect is normal to the film surface, the flux of J-vortex is also normal to the film surface. Hence the normal components of the flux at GB form J-vortices. Then what is the contribution of the parallel components of flux at GB for J_{cb} ? For this, Our data indicate very interesting features as following.

(3) Reduction factors for parallel fields

Since the field is almost parallel for Fig.2a, we take the average value of data for J_{cb} under parallel field of $\theta = 0°$ as shown by the center line (dotted line) in Fig.2a. The best fitting curve can be expressed by the following simple

Lorentzian reduction factor as a function of $H_\parallel$, while $H_\parallel = H_a$. The Lorentzian form is another form of modified Kim-Anderson model.

$$\frac{1}{1 + \alpha H_\parallel^2} \qquad (1)$$

where $\alpha = 1/0.36(1/KOe^2)$ and the unit of $H_\parallel$ is KOe . When $H_\parallel = H_a = 0$, J_{cb} becomes $J_0 = 0.59 \times 10^3 A/cm^2$. Hence the curve Fig.2a can be expressed by $\frac{J_0/1.8}{1 + \alpha H_\parallel^2}$. The solid line is obtained using the final formula expressed by Eq.(4) for the small $H_\perp$ for $\theta = 2°$
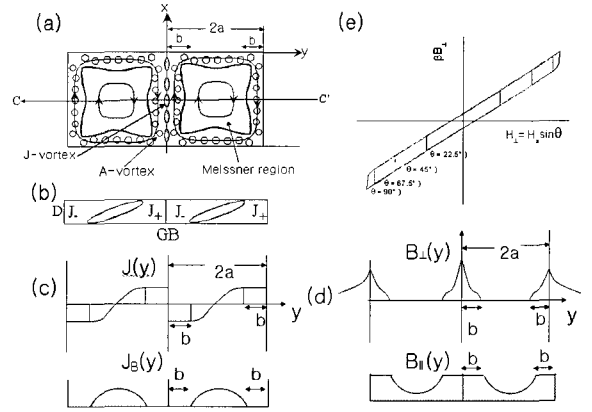

Fig. 4. Schematic diagrams to help understanding the concepts of our analyses for oblique H_a. (a) The top-view of the sample, where A-vortices, J-vortices, critical currents, and Meissner currents are shown. J-vortices are aligned at GB. The shielding currents, which consist of critical currents and Meissner currents, are circulating in the two domains without currents across GB. The Meissner currents circulate in the two Meissner regions. Similarly, the critical current circulates in each A-vortex region, which surrounds the Meissner region in each domain. (b) Cross-section of the thin film sample with the thickness, D. The two cores are shown, where no currents and no flux are formed. The shape of core is given in Ref.5 for the case of a single domain for a strip sample. The current densities are $\pm J_{cg}$ except the core regions [5]. (c) $J(y)$ is the distribution of critical currents and Meissner currents, which are integrations of current density over the thickness. $J(y)$ flows in x-direction in the cross-section CC' as shown in Fig.4a. "b" is the width of the A-vortex region for critical currents. $\pm J_B(y)$ are the screening currents for $H_\parallel$. More explanations are given in the text. (d) Distributions of the normal and the parallel components of magnetic flux, $B_\perp(y)$ and $B_\parallel(y)$. $B_\perp(y)$ is proportional to the density of A-vortices and vanishes in the Meissner regions. Notice the peak of $B_\perp(y)$ at GB, the square root of which is proportional to the density of J-vortices (the details are in

the text). (e) $\beta B_\perp$ vs $H_\perp$, which is calculated using Eq.(2) and shows the well known parallelogram. As θ increased, $\pm H_0$, which are the upper and the lower limit of $H_\perp$, are reduced. The y-coordinate and the x-coordinate of the intersection points are ± 0.79 and $\pm 71 Oe$, respectively.

(4) Reduction factors for normal fields

Fig.2e shows the well-known peaks with hysteretic curves for fields applied in normal direction, $H_\perp = H_a$. These can be explained by Brandt model [3]. Taking the edge field of a single strip for the field near GB, the average flux density at GB shows the well-known parallelogram [3](see Fig.4e), which can be calculated as following. The normal component of average flux intensity at GB is

$$B_\perp = \frac{\mu_0}{2\lambda}\int_{-\lambda}^{\lambda} dy H(y) \qquad (2)$$

Here $\lambda \approx 1000 nm$ is the penetration depth in ab-plane. The normal field for increasing $H_\perp$ can be rewritten [2][3]

as $H^\uparrow(y) = h(y)$, where

$$h(y) = 2H_c \tanh^{-1}[\frac{a(y^2 + 2ab - 2ay - b^2)^{1/2}}{(a-y)(2ab - b^2)^{1/2}}]$$

for $0 \le y \le b$, $H_c / D = J_{cg} / \pi$, and

$$a - b = a / \cosh(H_\perp / H_c)$$

Here D is the film thickness, 300nm and $4a = 10mm$ is the total length of sample. The intra-grain critical current density, J_{cg}, is $1.2 \times 10^6 A / cm^2$, which gives $H_c = 10 Oe$. The parameter, b, is the distance from GB to the boundary between the critical region and Meissner region (see Fig.4b, 4c, and 4d. The normal field for decreasing $H_\perp$ can be rewritten as $H^\downarrow = h(H_0, J_{cg}) + h(H_\perp - H_0, -2J_{cg})$. Here $\pm H_0$ is the upper and lower limit of $H_\perp$ for variation, which depends on θ.

Fig.4d shows the schematic diagram for the distribution of the normal components of fields, $B_\perp(y)$, which is proportional to the density of vortices. The film is divided into the Meissner region $(b \sim 2a - b)$ and the critical regions $(0 \sim b)$ and $(2a - b \sim 2a)$. In the Meissner region, the induced currents are not saturated (see Fig.4c) so that there is formed a flux-free and current-free region, so called core, which is formed between the upper and the lower regions with the currents of opposite directions (Fig.4b). In the critical regions, vortices penetrate with non-zero normal component of field with fully saturated constant current of J_{cg} (see Fig.4c) [3][5]. These two types of currents determine field distribution, especially the edge fields. For typical cases, the distance of A-vortex penetration from GB is $b \approx 0.3mm$ for $H_\perp \approx 10 Oe$. This is ~ 300 times larger than the penetration depth. This means that screening currents around GB are saturated by

the focused flux for very small $H_\perp$. Hence, there is no more screening near GB for additional $H_\parallel$. The calculated curve of $\beta B_\perp$ vs $H_\perp$ shows the well known parallelogram(the factor β is defined below) as shown in Fig.4e. The upper and the lower limit of field are $\pm H_0 = \pm 0.7 \sin\theta(KOe)$. As θ increased, H_0 is reduced. The y-coordinate and the x-coordinate of the intersection points are ± 0.79 and $\pm 71 Oe (H_\perp^*$ for the two peaks),

respectively. The density of J-vortex is proportional to $\sqrt{B_\perp}$ because the inter-distances of A-vortices near GB and the inter-distance of J-vortices are similar. The data for $\theta = 90°$ fit well to $J_0 /(1 + \beta | B_\perp |)$, which is Kim's model[9] with the parameter $\beta^{-1} = 7 \times 10^8 \phi_0 / cm^2$ as shown by the solid line in Fig.2e. Here $J_0 = 0.59 \times 10^3 A / cm^2$ and ϕ_0 is the quantum flux. The paths of $B_\perp$ for these cases are shown in Fig.4e. The basic parallelogram doesn't change, while the changing variable is H_0 only. The reduction factor for $H_\perp$ is

$$\frac{1}{1 + \beta | B_\perp |} \qquad (3)$$

The unit of $B_\perp$ is Gauss.

(5) Reduction factors for oblique fields

As the applied field is tilted from the normal direction, both $H_\parallel$ and $H_\perp$ are finite. Since there is no screening at GB for $H_\parallel$ and the parallel component of field given by Brandt model for $H_\perp$ vanish at GB by the symmetry for $\pm y$, the parallel component of flux intensity at GB is simply $B_\parallel = \mu_0 H_\parallel$. The normal component of flux intensity at GB, $B_\perp$, is given by the previous Brandt formula, Eq.(2).

We found that our data for oblique fields are well explained by the reduction factor, which is expressed by multiplying the two factor,

$$\frac{J_0}{(1 + \alpha H_\parallel^2)(1 + \beta | B_\perp |)} \qquad (4)$$

for general θ s. Here $J_0 = 0.59 \times 10^3 A / cm^2$ as before, of course. All the lines in Fig.2a, 2b, 2c, 2d, and 2e are obtained from this single formula. Even the curves in Fig.2a and Fig.2e also fit well to Eq.(4). When we take $H_\parallel = 0$, Eq.(4) becomes $J_0 /(1 + \beta | B |)$, which is the same as that in section (4). And, when we take a very small value of $\theta \approx 2°$, the factor of Eq.(4) becomes $\frac{1}{1 + \beta | B |} \approx 1 / 1.8$ as the parallelogram for βB converges to ± 0.79. Then Eq.(4) becomes $\frac{J_0 / 1.8}{1 + \alpha H_\parallel^2}$, which is the

same as that in section (3). The solid line in Fig.2a is obtained from Eq.(4) with the small hysteretic curves. It is also explained why Fig.2a does not show peaks. Hence, all the data in Fig.2 successfully fit well to Eq.(4). The differences and the similarities of J_{cb} s at the crossing points ($H_a = 0$), the peak points, and the tails of curves fit well to this equation at a time.

It is remarkable that all of the five data sets in Fig.2a, 2b, 2c, 2d, and 2e are explained by a single equation with the same parameters. The only variable is the angle, θ. This means that our concept for the explanation seems to be very meaningful.

4.   CONCLUSION

We measured critical current densities (J_{cb}) at the 30° grain boundary of a bicrystalline $(Sm_{0.8}Dy_{0.2})Ba_2Cu_3O_7$ film under various magnetic fields($\overrightarrow{H}_a$), which were applied obliquely. We varied the field from $-0.7KOe$ to $+0.7KOe$ while the angles(θ) of the fields were 2°, 22.5°, 45°, 67.5° and 90° with respect to the film surface. The curves of J_{cb} vs $\overrightarrow{H}_a$ showed the well known butterfly-like hysteretic curves. We separated the field into the two components, $H_\perp$ and $H_\parallel$, which are normal and parallel to the film surface, respectively. We applied Brandt model for the response of vortex distribution to $H_\perp$. We found Lorentzian factor is good enough to explain the experimental feature for $H_\parallel$. We combine the effect of

$H_\perp$ deduced from the data of $\theta = 90°$ and the effect of $H_\parallel$ deduced from the data of $\theta = 90°$ by multiplication of the two different reduction factors. All data for general θ s fit well to this new factor. This means that our concept for explanation seems to be very meaningful and all the data have self-consistency within the regime of our concept.

REFERENCES

[1]   J.Hanisch, V.S.Sarma, B.Zeimetz, F.Schindler, J.Eickemeyer, L.Schultz, B.Holzapfel, *Supercond. Sci. Technol.* 17 (2004) 1003

[2]   H.S.Kim, B.S.Lee, K.C.Chung, S.M.Lim, D.Youm, *Physica C* 397 (2003) 19 ; K.C.Chung, E.S.Lee, B.S.Lee, S.M.Lim, S.I.Bhang, and D. Youm, *Supercond. Sci. Technol.* 17 (2004) 1113

[3]   E.H.Brandt and M.Indenbom, *Phys. Rev. B* 48 (1993) 12893

[4]   D.Goo, K.Jung, H.Kim, and D.Youm, *Supercond. Sci. Technol.* 13 (2000) 1569

[5]   G.P.Mikitik, E.H.Brandt, and M.Indenbom, *Phys. Rev. B* 70 (2004) 014520

[6]   B.S.Lee, K.C.Chung, H.S.Kim, S.M.Lim, and D.Youm, *Supercond. Sci. Technol.* 17 (2004) 493

[7]   A.Badia, C.Lopez, J.L.Giordano, *Phys. Rev. B* 58 (1998) 9440

[8]   C.P.Bean, *Phys. Rev. Lett.* 8 (1962) 250, *Rev. Mod. Phys.* 36 (1964) 31

[9]   Y.B.Kim, C.F.Hempstead, and A.R.Strand, *Phys. Rev.* 129 (1963) 528, *Phys. Rev. Lett.* 9 (1962) 306